Copper Nanocubes for CO₂ Reduction in Gas Diffusion Electrodes

Yuxuan Wang,^{1,†} Hao Shen,^{1,†}, Ken J. T. Livi,² David Raciti,³ Han Zong,¹ John Gregg,¹
Mofopefoluwa Onadeko,¹ Yidong Wan,¹ Adam Watson,¹ and Chao Wang^{1,*}

¹Department of Chemical and Biomolecular Engineering and ²Department of Materials Science and Engineering, Johns Hopkins University, Baltimore, Maryland 21218, United States

³Materials Science and Engineering Division, National Institute of Standards and Technology, Gaithersburg, Maryland 20899, United States

*Email: chaowang@jhu.edu.

[†]Equal contributions.

Abstract: Electroreduction of CO₂ represents a promising solution for addressing the global

challenges in energy and sustainability. The reaction is highly sensitive to the surface structure of

electrocatalysts and the local electrochemical environment. We have investigated the effect of Cu

nanoparticle shape on the electrocatalysis of CO₂ reduction by using gas-diffusion electrodes

(GDEs) and flowing alkaline catholytes. Cu nanocubes of ~70 nm in edge length are synthesized

with {100} facets preferentially exposed on the surface. They are demonstrated to possess

substantially enhanced catalytic activity and selectivity for CO₂ reduction as compared to Cu

nanospheres of similar particle sizes, with the electrocatalytic performance further found to be

dependent on the concentration of electrolyte (KOH). The Cu nanocubes reach a Faradaic

efficiency (FE) of 60% and a partial current density of 144 mA/cm² toward ethylene (C₂H₄)

production, with the catalytic enhancement attributable to a combination of surface structure and

electrolyte alkalinity effects.

Keywords: CO₂ reduction, copper electrocatalysts, shape, gas diffusion electrode, ethylene

2

Electroreduction of CO₂ represents a promising approach toward artificial carbon recycling and solar-fuel conversion.¹⁻³ Among the many materials investigated for CO₂ reduction, copper (Cu) has attracted the most attention due to its unique capability of producing hydrocarbon products at significant rates.⁴⁻⁷ The reaction is highly sensitive to the surface structure of Cu, with (100) favoring the production of ethylene and (110) for oxygenated hydrocarbons such as ethanol and acetic acid.⁸⁻¹² The unique four-fold symmetry of atomic configurations on these Cu facets is likely the key to accommodate the transition state of C-C bond formation between adsorbed CO (*CO), giving rise to more favorable kinetics for the pathways toward C₂ products than on Cu(111).¹³ All of these fundamental insights point to the importance of controlling the morphology and thereby surface structure of Cu electrocatalysts for selective reduction of CO₂ to valuable C₂ products.⁷

The electrocatalytic performance of Cu in CO₂ reduction is however not only determined by its surface structure, but also by the local electrochemical environment. The CO₂ reduction reaction, as well as the side hydrogen evolution reaction (HER), generates hydroxide anions and raise the local pH near the electrode surface. The high local pH could play a complex role in the CO₂ reduction electrocatalysis, being either beneficial by suppressing the evolution of hydrogen and enhancing the selectivity toward C₂ products, ¹⁴⁻¹⁸ or detrimental by shifting the acid-base reaction equilibrium of (bi)carbonate and limiting the mass transfer of CO₂¹⁹⁻²¹. The performance of CO₂ electrolyzers can also be subject to spatial geometry of the electrodes, ²²⁻²⁵ ions and/or ligands present at the electrochemical interface, ^{19, 26-28} bulk pH and buffering strength of the electrolyte, ^{17, 29-30} (partial) pressures of the reactant and products, ³¹⁻³² fluidics of the gas and liquid, ³³⁻³⁴ local effect of catalyst areal density, ³⁵⁻³⁶ etc. For fundamental understanding of the structure-property relationships of high-surface-area electrocatalysts, it is important to decouple these mechanisms from the surface structure effects in studying the electroreduction of CO₂. ³⁷

Here we report on the electrocatalytic study of particle shape effect on CO_2 reduction using gas-diffusion electrodes (GDEs). Cubic Cu nanocrystals of ~70 nm in edge length were synthesized with preferential exposure of $\{100\}$ facets on the surface. Cu nanoparticles of similar particle sizes but in a sphere-like shape were also synthesized for comparative studies. By employing GDEs with flowing alkaline catholytes, we were able to evaluate the electrocatalytic performance of these Cu nanocrystals without concerning the mass transfer limitation and local pH effects (Scheme 1), while still achieving high selectivity toward C_2 products. Comparison of the two types of Cu nanocrystals thus allows us to reveal the effects of particle morphology and surface structure on the CO_2 reduction electrocatalysis.

The Cu nanocubes were synthesized by following a previously reported method (see the Experimental Methods in the Supporting Information). Figure 1a shows a representative transmission electron microscopy (TEM) image of the as-synthesized Cu nanocubes. The uniform Cu nanocrystals possess an edge length of ~70 nm (see Figure S1 for the size histograms), forming assemblies with a four-fold symmetry due to the uniform cubic shape. Figure 1b compares the X-ray diffraction patterns for the Cu nanocubes to the Cu nanospheres of similar particle size but in a sphere-like shape (see Figure S2 for TEM images). Both the two types of nanocrystals possess a face-centered cubic phase of metallic Cu. Compared to the nanospheres, the nanocubes exhibit a much more pronounced (200) peak than (111), which can also be attributed to the formation of cubic assemblies and confirm the uniform shape of the nanocrystals. To depict the surface structure of the nanocrystals, we collected high-resolution TEM (HRTEM) images along the [011] zone axis by tilting the sample holder (Figures 1c and d). The HRTEM images show lattice fringes corresponding to (100) and (110) of Cu with inter-layer distances of 0.18 and 0.13 nm, respectively. As expected, the surface facets of the nanocubes are identified to be (100), albeit exposure of some

other planes (such as (110) and (111)) probably around the corners and edges. It should be pointed out here that direct imaging along [001] was found to be challenging, due to the rather thick crystal for the electron beam to penetrate in this direction. The distinct surface structures of the Cu nanocubes and nanospheres were further confirmed with OH⁻ adsorption measurements, with only the Cu nanocubes showing the pronounced feature of Cu(100) (Figure S3).

Electrocatalytic studies were performed on the Cu nanocrystals by employing a GDE cell design developed by Whipple et al (Figure S4).³³ Ligands on the Cu nanocubes were cleaned by extensive washing with ethanol/toluene mixture but more violent methods (such as thermal annealing in air) were avoided in order to preserve the cubic shape and surface structure of the Cu nanocrystals.³⁹⁻⁴⁰ The Cu nanocrystals dispersed in hexane were sprayed directly onto a microporous gas diffusion layer (GDL) (purchased from the Freudenberg Group), which was then applied as the working electrode for CO₂ reduction (Scheme 1). CO₂ was fed into the cell by flowing through the backside of the GDL. Liquid electrolyte (KOH) was flown through the cathode compartment between the catalyst and the anion-exchange membrane (Fuel Cell Store, Fumasep FAB-PK-130). The gas- and liquid-phase products were analyzed online by using a gas chromatography-mass spectrometry (GC-MS) and offline by using a nuclear magnetic resonance (NMR) spectrometer, respectively. Measurements were performed in the potential region from -0.3 to -0.8 V (vs. the reversible hydrogen electrode, RHE; the same potentials scale is used throughout this discussion), which corresponds to ca. -0.30~ -0.72 V after iR correction (see Table S1 for the estimated resistances). The absence of mass transfer limitation in the GDE was confirmed by measurements at different gas and liquid flow rates (Figure S5).

Figure 2 summarizes the results collected by using 1 M of KOH as the catholyte (see Figure S6 for the iR-corrected version). The Cu nanocubes and nanospheres show similar trend in total

geometric current densities (Jtot). As the potential changes from -0.3 to -0.8 V, Jtot of Cu nanospheres increases from 1.6 mA/cm²_{geo} to 130 mA/cm²_{geo}, while that for Cu nanocubes changes from 4.3 mA/cm²_{geo} to 160 mA/cm²_{geo} (Figures 2a and c). Potential-dependent Faradaic efficiencies (FEs) of the reaction products are plotted in Figures 2b and d for the Cu nanocubes and nanospheres, respectively. For the Cu nanocubes, the overall FE of CO₂ reduction (FE_{CO2}) is consistently at 70 – 90% throughout the investigated potential region. CO is the dominant product at relatively low overpotentials (from -0.3 to -0.5 V), with FE_{CO} being up to 70% at -0.3 V. As the potential becomes more negative, FE_{CO} decreases, down to 24% at -0.8 V. This is accompanied with the rise of C₂ products formation, with the FE toward ethylene (FE_{C2H4}) increasing from 14% at -0.6 V to 51% at -0.8 V. The catalysts collected after the reaction preserved the cubic morphology (Figure S7), indicating high stability of the 70 nm Cu nanocubes under the CO₂ reduction reaction conditions. The electrocatalytic performance of the Cu nanocubes was also found to be stable for continuous operations of up to 3 h (at -0.6 V in 1 M KOH, Figure S8). It is noticed that nanoparticle restructuring and loss of activity may take place when subjected to longer runs and more negative potentials. 41 Compared to the Cu nanocubes, the Cu nanospheres exhibit slightly lower FE_{CO2} in the low-overpotential region, ranging from 52% at -0.3 V to 81% at -0.5 V. Formate is the primary product in this potential region, with FE_{HCOO}⁻ being up to 55% at -0.5 V. In the high-overpotential region (from -0.6 to -0.8 V), the nanospheres also have FE_{CO2} in the range of 80-90%, but produce less C₂ species, with FE_{C2H4} and the total FE toward C₂ products (FE_{C2}) being up to only 20% and 27% at -0.8 V, respectively.

We note that most of the previous studies for CO₂ reduction on Cu nanocrystals of similar morphologies were performed in H-type electrochemical cells with bicarbonate electrolytes.⁴²⁻⁴⁵ In an investigation of Pd@Cu core@shell nanocubes, Z. Wang *et al.* found CH₄ as the dominant

hydrocarbon product (~45% FE at -1.4 V in 0.25 M K₂CO₃).⁴³ A. Loiudice *et al.* evaluated the Cu nanocubes of different sizes in 0.1 M KHCO₃ and obtained FE_{C2H4} as high as 41% at -1.1 V.⁴⁴ In our electrocatalytic studies using GDEs, we were able to obtain much larger fluxes of CO₂ reduction products at lower overpotentials. We achieved J_{CO2} of 153 mA/cm²_{geo} at -0.8 V for the Cu nanocubes (Figure 2a), versus the highest J_{CO2} of <5 mA/cm²_{geo} obtained at -1.1 V in the previous studies using H-type cells.⁴⁴ This enhancement is not only due to the mitigation of mass transfer limitation, but also the employment of flowing alkaline electrolytes, which is believed to be beneficial for suppressing hydrogen evolution, lowering the energy barrier for CO₂ activation and enhancing C-C coupling between *CO.^{16, 23, 29, 33, 46-48} To further elucidate this beneficial role, we have also performed the electrocatalytic studies using more concentrated KOH electrolytes and 1 M of KHCO₃ as the flowing catholyte (see Figure 3 for 10 M of KOH, with iR-corrected version provided in Figure S9; see also Figure S10 for 5 M of KOH).

The Cu nanocubes deliver 259, 219 and 144 mA/cm 2 _{geo} for J_{tot}, J_{CO2} and J_{C2H4} at -0.8 V, respectively, when 10 M KOH was used as the electrolyte (Figure 3a). The onset potential for hydrocarbons are lowered by more than 300 mV than in the case using 1 M KOH, with FE_{C2H4} reaching 23% at -0.3 V and J_{C2H4} reaching 46 mA/cm 2 _{geo} at -0.5 V (Figure 3b). The selectivity toward C₂ products is also enhanced by increasing the electrolyte alkalinity, with FE_{C2H4} achieving 60% at -0.5 V and FE_{C2} being up to 72% at -0.7 V. Electrocatalytic performance of the Cu nanospheres got improved as well when the electrolyte was changed from 1 M to 10 M KOH (Figure 3c and d). J_{tot} reaches 174 mA/cm 2 _{geo} at -0.8 V. The production of formate is suppressed in the low-overpotential region, with the highest FE_{HCOO}- being 35% at -0.3 V. The selectivity toward C₂ species (FE_{C2}) achieves 60% at -0.8 V, which is substantially higher than that (27%) obtained with 1 M of KOH. Compared to the Cu nanocubes, the Cu nanospheres produce more

acetate at high overpotentials in 10 M of KOH, with FE_{CH3COO}⁻ reaching 26% (versus 38% for FE_{C2H4}) at -0.6 V. For both Cu nanocubes and nanospheres, the trends for total current densities and partial current densities toward C₂ products follow the trend 1M KOH < 5M KOH < 10M KOH, underlining a strong correlation between KOH concentration and activity of CO₂ reduction to C₂ products (Figure S11). This trend is consistent the report by Dinh et al. who used GDEs with polycrystalline Cu films prepared by thermal evaporation.²³ In contrast to the enhanced activity and selectivity by increasing the concentration of KOH, (oxygenated) hydrocarbons were barely obtained from the measurements employing 1 M of KHCO₃ (pH ~ 8.9, not saturated with CO₂ in GDEs), from which H₂, CO and formate were the major products throughout the potential range of -0.8 V \leq E \leq -0.3 V (Figure S12). CO is the dominant product on the Cu nanocubes, with FE_{CO} ranging from 30% at -0.3 V to 50% at -0.8 V, comparing to 8-26% for the Cu nanospheres within the same potential range. Given with the substantially higher activity and selectivity obtained with KOH than with neutral KHCO₃, it should be noted that the employment of alkaline electrolytes in GDEs may lead to the formation of bicarbonate, although it has been argued that the short diffusion distance for CO2 in the GDEs can allow for reduction reaction before it is converted into bicarbonate.²³ While specific study of alkaline electrolyte degradation has not been seen in the literature, several reports have discussed the use of anion-exchange membrane (AEM)-based electrolyzers to mitigate this issue. 49-50

For better evaluation of the intrinsic differences in electrocatalytic performance, we have performed electrochemical analyses to estimate the electrochemically active surface areas (ECSAs) for the two types of Cu nanocrystals (see Experimental Method in the Supporting Information). This was achieved by measuring the charge associated with surface oxidation of Cu to Cu₂O.⁵¹⁻⁵² It is considered to be an appropriate method for the Cu nanocrystals loaded on the carbon-based

GDLs, as other methods (e.g., electrochemical capacitance measurements⁵³) are usually subject to the large background signal of the high-surface-area substrates. At the same metal loading (1 mg_{Cu}/cm²_{geo}), the ECSAs of the Cu nanocubes and nanospheres were estimated to be 7.89 and 9.09 cm², respectively (Figure S13). With the estimated ECSAs, we are then able to compare the specific activities (current densities normalized with ECSAs) for the two types of Cu nanocrystals.

Figure 4 summarizes the specific activities determined for the Cu nanocubes and nanospheres in 10 M of KOH. The Cu nanocubes deliver an overall specific activity (j_{tot}) of 32 mA/cm²_{Cu}, versus 19 mA/cm²_{Cu} for the Cu nanospheres, at -0.8 V (Figure 4a). The Cu nanocubes are found to be more active than the Cu nanospheres for CO₂ reduction throughout the investigated potential region, with j_{CO2} reaching 28 mA/cm²_{Cu} (versus 15 mA/cm²_{Cu} for the Cu nanospheres) at -0.8 V (Figure 4b). The different selectivities of the two types of Cu nanocrystals toward C₂ products become explicit by comparing the specific activities toward ethylene (j_{C2H4}) and acetic acid (j_{CH3COO}-). The Cu nanocubes give rise to 5.8 mA/cm²_{Cu} for j_{C2H4} at -0.5 V, which represents an improvement factor of ~3.4 versus the Cu nanospheres (1.7 mA/cm²_{Cu}) at this potential. The nanospheres produce slightly more acetate in the low-overpotential region (-0.5 V and more positive potentials), but j_{CH3COO}- becomes rather similar at higher overpotentials. Our results thus emphasize the importance of controlling both catalyst structures and reaction conditions to improve the reactivity and selectivity of CO₂ reduction.

From the above discussion, we can see that the Cu nanocubes are both more active and selective than the Cu nanospheres for reduction of CO₂ to ethylene in alkaline electrolytes. This catalytic enhancement can be ascribed to the preferential exposure of (100) facets on the surface of the Cu nanocubes as compared to the Cu nanospheres. Cu(100) is known for favoring direct coupling of *CO and production of ethylene in CO₂ and CO reduction. This pathway has a

lower energy barrier than the C-C coupling via *CHO (intermediate formed by hydrogenation of *CO), the situation likely accountable for the formation of C₂ products on Cu(111) at relatively high overpotentials. ^{58, 48} The pathway via direct coupling of *CO is mediated by electron transfer and pH-dependent on the RHE scale, giving rise to positive shift of onset potential at increasing electrolyte pH. ¹¹ This mechanism explains the further enhanced catalytic activity and selectivity of the Cu nanocubes in more concentrated KOH (5 and 10 M). It is interesting that the concentration of KOH plays a more substantial role in the case of Cu nanospheres than on Cu nanocubes. This could be ascribed to the intrinsically higher barrier for C-C coupling on Cu(111) than on Cu(100), leaving larger space for improvement by tuning the alkaline concentration. ¹⁰

Debates are still present in the literature about acetate production from CO₂ reduction on Cu electrocatalysts. Luc *et al.* argued acetate is more favorably produced on Cu {111} in CO reduction, due to the suppression of other C₂ product, such as ethylene and ethanol.⁵⁹ Hahn *et al.* reported that the competitive adsorption of *CO and *H makes undercoordinated stepped surfaces like (751) more selective for oxygenates at low over-potentials.⁶⁰ Our results show that, while C-C coupling and ethylene formation is sensitive to the catalyst surface structure, acetate production is quite less. The latter might be explained by the mechanism reported by Luc *et al.* that the incorporation of water into ketene-like intermediate such as ethenone (CH₂–CO) to form acetic acid is not sensitive to the Cu surface structure due to the very weak binding of this C₂ intermediate (0.06 eV on Cu(111) versus 0.21 eV on Cu(100)).

Formation of *CO, as well as the corresponding desorption product CO(g) and further reduced C₂ products (through C-C coupling) originates from a carboxyl adsorbate (*COOH) after activation of CO₂, whereas formate can be generated from either *COOH or *HCOO (adsorbed formate).⁶¹⁻⁶² Formate production is much more favorable on Cu{111} via the *HCOO pathway

than on Cu{100} via either *HCOO or *COOH. This explains the more preferential production of formate at relatively low overpotentials (e.g., more positive than -0.5 V in 1 and 10 M KOH) on Cu nanospheres than on Cu nanocubes (Figures 2 and 3), which is also consistent with the report on Cu single crystals.^{8, 12} For example, in the study of Huang et al., CO is the main product of CO₂ reduction on Cu(100) at potentials more positive than -0.6 V (FE_{CO} < 10%), whereas formate is the major product on Cu(111) at potentials more positive than -1.0 V (FE_{formate} up to 20% versus <10% for FE_{CO}). 12 The low-overpotential production of formate at significant rates is also consistent with the reports on Cu electrocatalysts using H-type cells. ^{59, 63-64} At high overpotentials, formation of *CO becomes feasible on both Cu{111} and Cu{100}, but C-C coupling between *CO is more favorable on Cu{100} than on Cu{111}, giving rise to the higher activity of Cu nanocubes than Cu nanospheres toward C₂ products (see comparison of j_{C2H4} in Figure 4c). It should be pointed out that formate was not observed in significant amounts from the previous GDE studies of CO₂ reduction on Cu-based electrocatalysts.^{23, 46} Although there is usually a lack of surface structure information, we hypothesize that the highly polycrystalline and disordered catalysts employed in the previous studies are abundant with surface defects (e.g., high-angle grain boundaries, steps and corners), which may give rise to dissimilar catalytic behaviors from the Cu nanocrystals of single-crystal nature as investigated here.

In summary, we have performed comparative electrocatalytic study of CO₂ reduction on Cu nanocubes and nanospheres by using gas-diffusion electrodes with flowing alkaline catholytes. The Cu nanocubes were found to exhibit enhanced catalytic activity for reduction of CO₂ to ethylene as compared to the Cu nanospheres. The electrocatalytic performance was further improved by using more concentrated alkaline catholyte. Our work highlights the importance of

controlling both surface structure and electrochemical environment for improving the energy

conversion and chemical transformation efficiencies of CO₂ reduction.

Corresponding Author

*E-mail: chaowang@jhu.edu

Author Contributions

†Y.W. and H.S. contributed equally. The manuscript was written through contributions of all

authors. All authors have given approval to the final version of the manuscript.

Notes. The authors declare no competing financial interests.

Acknowledgements. This work was supported by the National Science Foundation (CHE-

1437396 and CBET-1803482). The authors also acknowledge The Catalyst and Discovery Awards

of Johns Hopkins University. This study made use of the Johns Hopkins University Department

of Chemistry Core Facilities and the authors would like to acknowledge the NMR manager Dr.

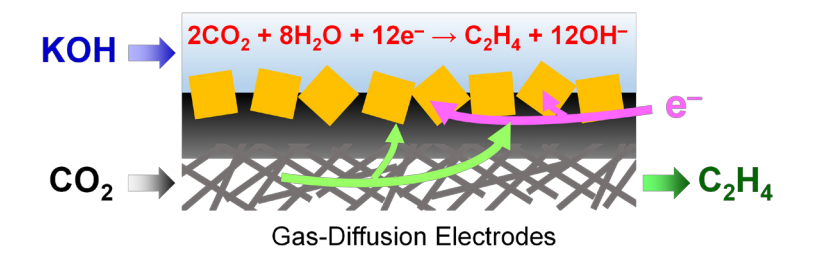
Joel A. Tang for his assistance. The authors also acknowledge Prof. Tyrel McQueen (Dept.of

Chemistry, JHU) and his student Hector Vivanco for assistance on XRD analysis.

Scheme 1. Illustration of the GDE employed for electrocatalytic studies of CO₂ reduction on the

truncated Cu nanocubes.

12



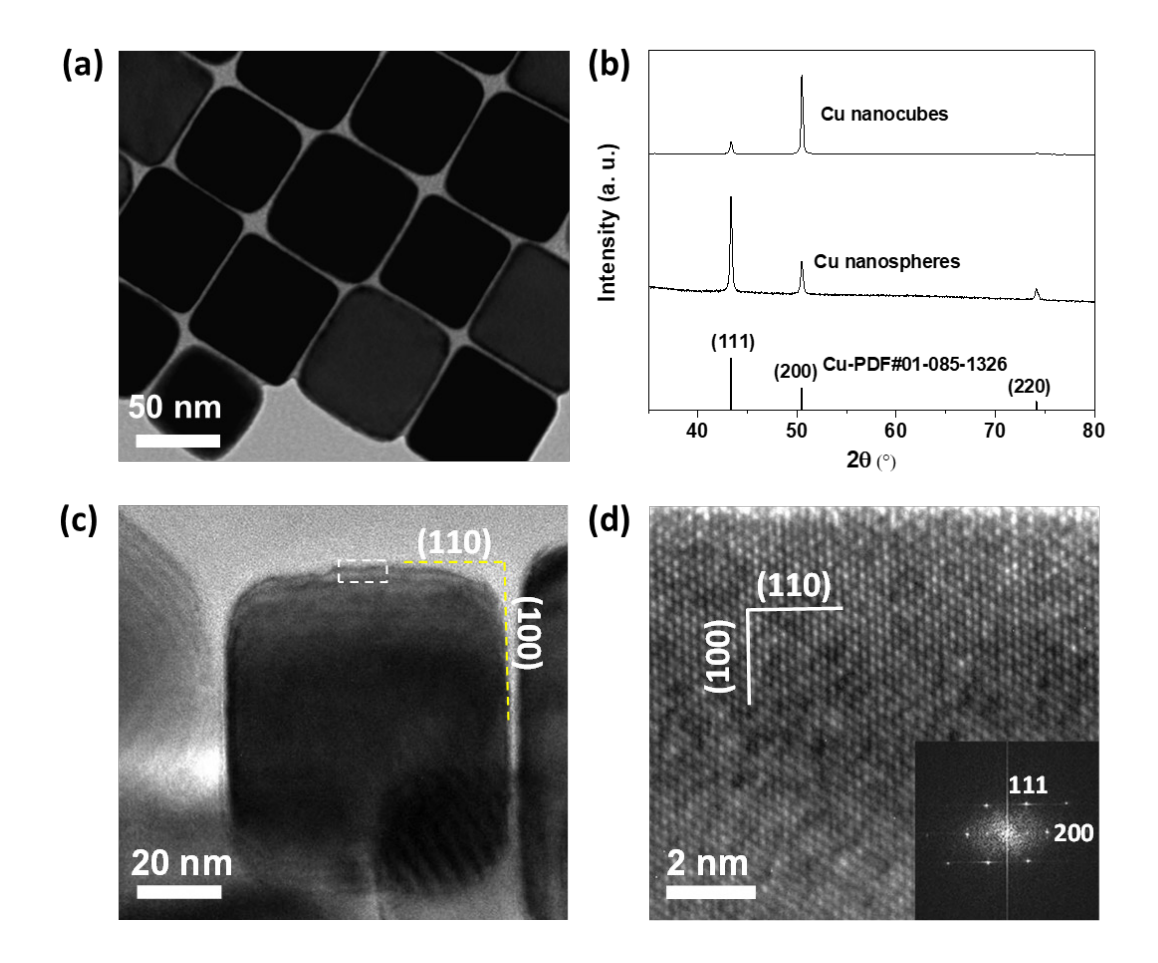


Figure 1. (a) Representative TEM image of Cu nanocubes. (b) Powder X-ray diffraction patterns collected on the Cu nanocubes and nanospheres. (c, d) HRTEM images taken along the $[0\bar{1}1]$ zone axis on a Cu nanocube. To reduce the penetration depth for electron beam, (d) is collected from the edge of the tilted nanocube, as labeled by the white dash box shown in (c).

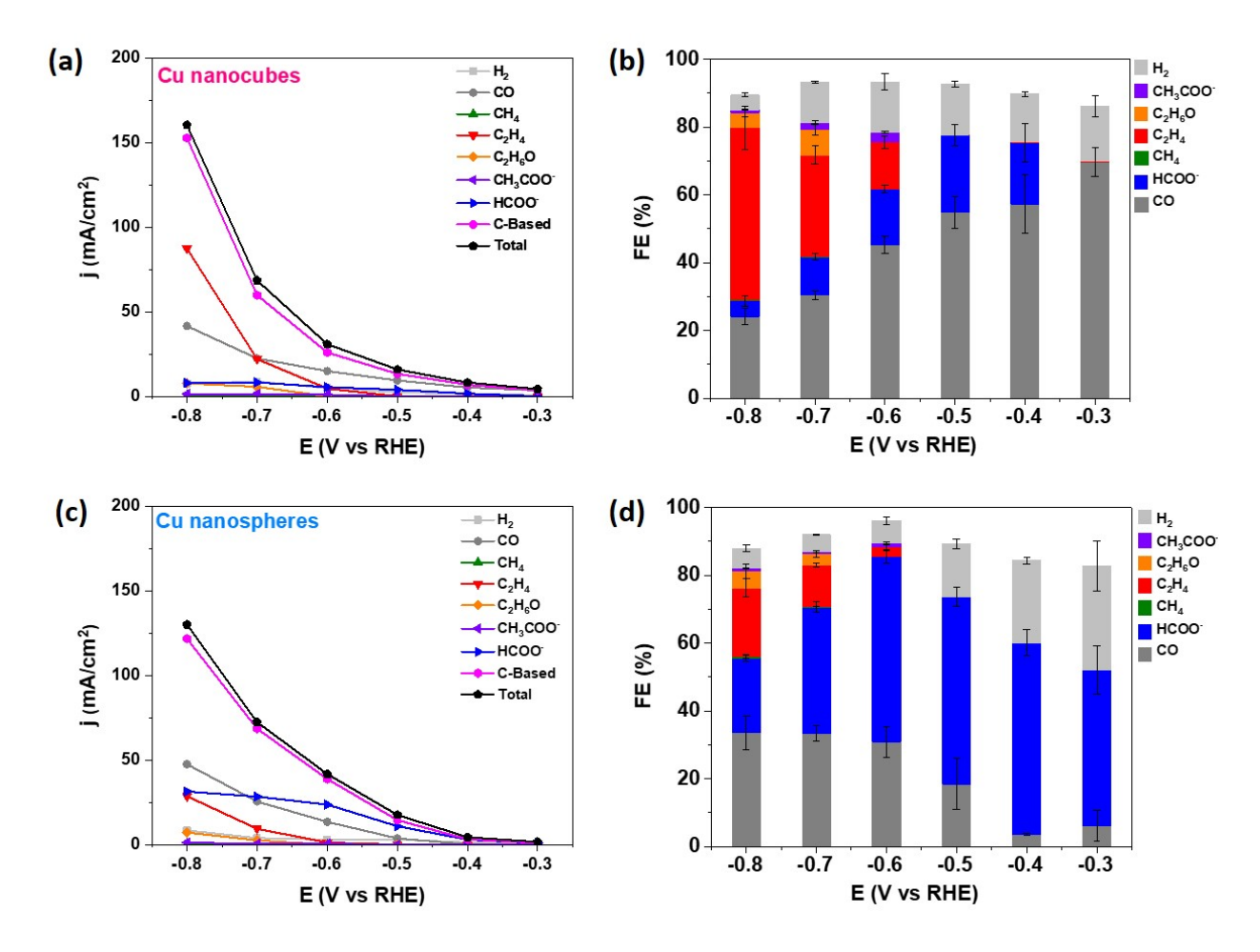


Figure 2. (a) Total electrode current densities (J_{tot} , per geometric area) and (b) Faradaic efficiencies (FEs) measured for the Cu nanocubes by using 1 M of KOH as the catholyte. (c, d) Corresponding results for the Cu nanospheres.

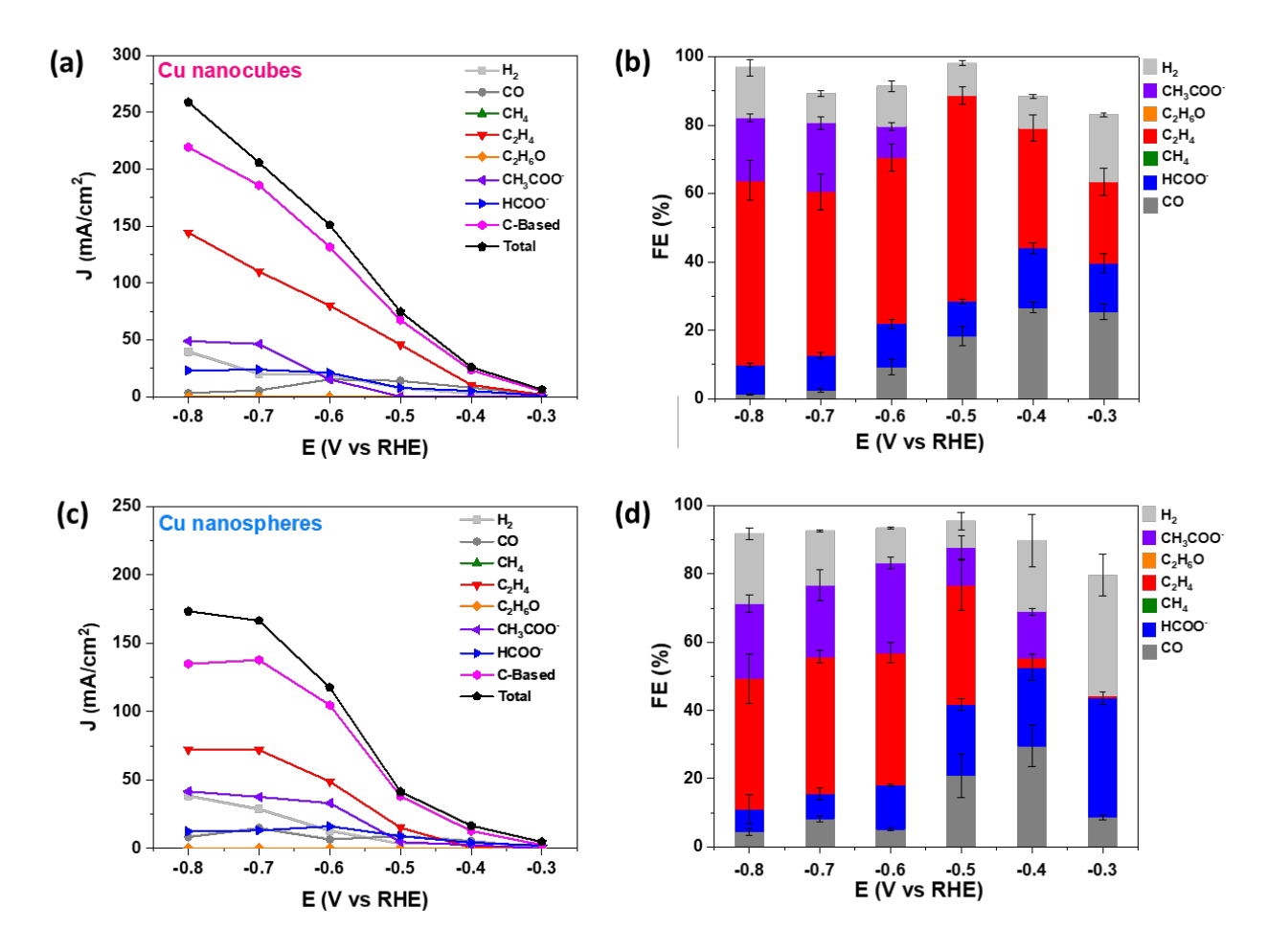


Figure 3. (a) Total electrode current densities (J_{tot} , per geometric area) and (b) Faradaic efficiencies (FEs) measured for the Cu nanocubes by using 10 M of KOH as the catholyte. (c, d) Corresponding results for the Cu nanospheres.

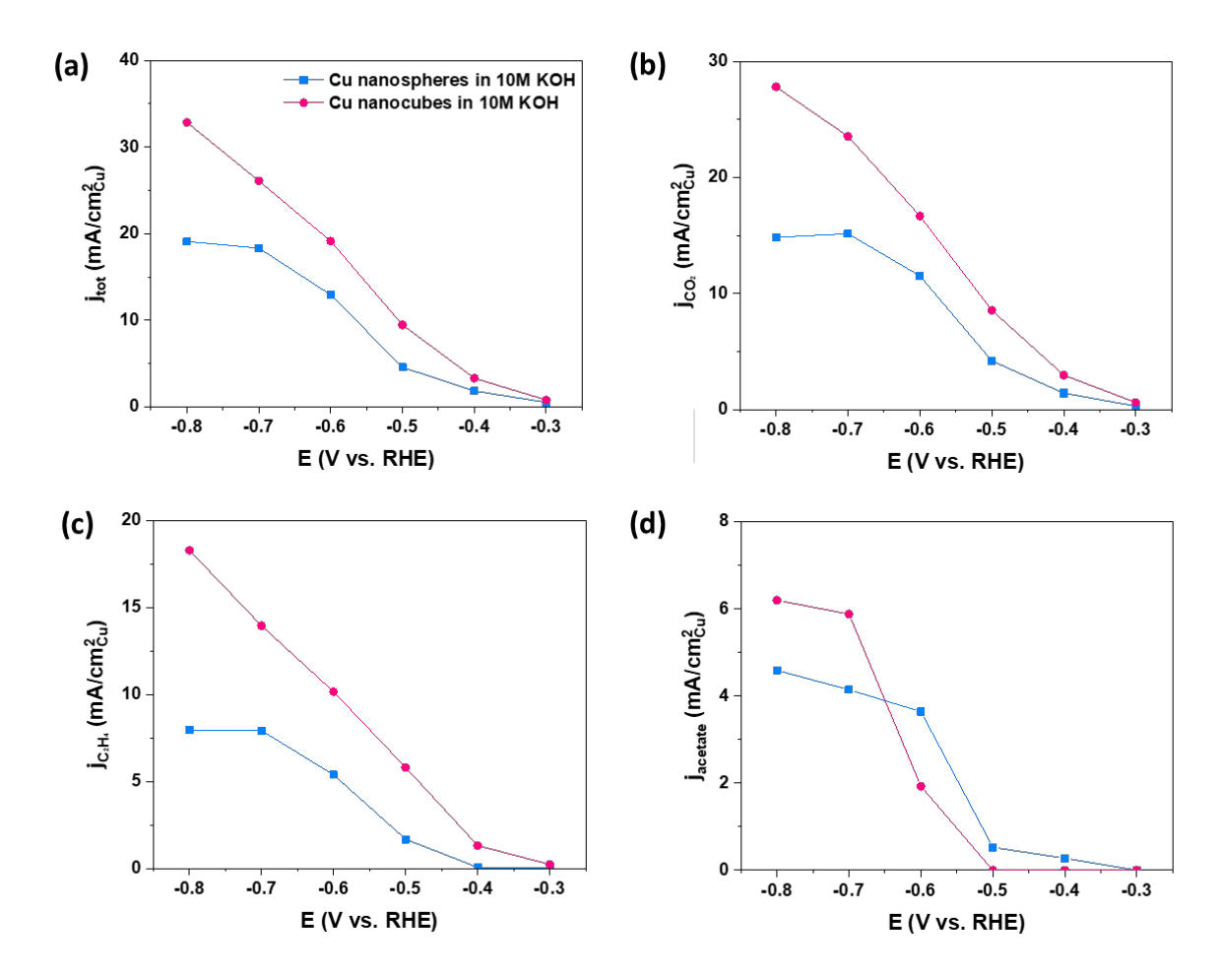


Figure 4. Comparison of specific activities for the two types of Cu nanocrystals in 10 M of KOH: (a) total current densities (j_{tot}); (b) current densities for CO₂ reduction by counting all the carbonaceous products (j_{CO2}); (c) partial current densities for ethylene production (j_{C2H4}); (d) partial current densities toward acetate (j_{CH3COO}⁻).

Reference

- 1. Whipple, D. T.; Kenis, P. J. A., Prospects of CO₂ Utilization via Direct Heterogeneous Electrochemical Reduction. *J. Phys. Chem. Lett.* **2010**, *1* (24), 3451-3458.
- 2. Mikkelsen, M.; Jørgensen, M.; Krebs, F. C., The teraton challenge. A review of fixation and transformation of carbon dioxide. *Energy Environ. Sci.* **2010**, *3* (1), 43-81.
- 3. Olah, G. A.; Prakash, G. K. S.; Goeppert, A., Anthropogenic Chemical Carbon Cycle for a Sustainable Future. *J. Am. Chem. Soc.* **2011**, *133* (33), 12881-12898.
- 4. Hori, Y.; Kikuchi, K.; Suzuki, S., Production of CO and CH₄ in Electrochemical Reduction of CO₂ at Metal-Electrodes in Aqueous Hydrogencarbonate Solution. *Chem. Lett.* **1985**, (11), 1695-1698.
- 5. Hori, Y., Electrochemical CO₂ Reduction on Metal Electrodes. *Modern Aspects of Electrochemistry*, No 42 **2008**, (42), 89-189.
- 6. Kuhl, K. P.; Hatsukade, T.; Cave, E. R.; Abram, D. N.; Kibsgaard, J.; Jaramillo, T. F., Electrocatalytic Conversion of Carbon Dioxide to Methane and Methanol on Transition Metal Surfaces. *J. Am. Chem. Soc.* **2014**, *136* (40), 14107-14113.
- 7. Raciti, D.; Wang, C., Recent Advances in CO₂ Reduction Electrocatalysis on Copper. *ACS Energy Letters* **2018**, *3* (7), 1545-1556.
- 8. Hori, Y.; Takahashi, I.; Koga, O.; Hoshi, N., Electrochemical reduction of carbon dioxide at various series of copper single crystal electrodes. *J. Mol. Catal. A: Chem.* **2003**, *199* (1), 39-47.
- 9. Schouten, K. J. P.; Gallent, E. P.; Koper, M. T. M., Structure Sensitivity of the Electrochemical Reduction of Carbon Monoxide on Copper Single Crystals. *ACS Catal.* **2013**, *3* (6), 1292-1295.
- 10. Raciti, D.; Cao, L.; Livi, K. J. T.; Rottmann, P. F.; Tang, X.; Li, C.; Hicks, Z.; Bowen, K. H.; Hemker, K. J.; Mueller, T.; Wang, C., Low-Overpotential Electroreduction of Carbon Monoxide Using Copper Nanowires. *ACS Catal.* **2017**, *7* (7), 4467-4472.
- 11. Schouten, K. J. P.; Qin, Z.; Pérez Gallent, E.; Koper, M. T. M., Two Pathways for the Formation of Ethylene in CO Reduction on Single-Crystal Copper Electrodes. *J. Am. Chem. Soc.* **2012**, *134* (24), 9864-9867.
- 12. Huang, Y.; Handoko, A. D.; Hirunsit, P.; Yeo, B. S., Electrochemical Reduction of CO₂ Using Copper Single-Crystal Surfaces: Effects of CO* Coverage on the Selective Formation of Ethylene. *ACS Catal.* **2017**, *7* (3), 1749-1756.
- 13. Li, H. J.; Li, Y. D.; Koper, M. T. M.; Calle-Vallejo, F., Bond-Making and Breaking between Carbon, Nitrogen, and Oxygen in Electrocatalysis. *Journal of the American Chemical Society* **2014**, *136* (44), 15694-15701.
- 14. Hori, Y.; Murata, A.; Takahashi, R., Formation of Hydrocarbons in the Electrochemical Reduction of Carbon-Dioxide at a Copper Electrode in Aqueous-Solution. *J. Chem. Soc. Faraday Trans.* **1989,** *85*, 2309-2326.
- 15. Gupta, N.; Gattrell, M.; MacDougall, B., Calculation for the cathode surface concentrations in the electrochemical reduction of CO₂ in KHCO₃ solutions. *J. Appl. Electrochem.* **2006**, *36* (2), 161-172.
- 16. Varela, A. S.; Kroschel, M.; Reier, T.; Strasser, P., Controlling the selectivity of CO₂ electroreduction on copper: The effect of the electrolyte concentration and the importance of the local pH. *Catal. Today* **2016**, *260*, 8-13.
- 17. Kas, R.; Kortlever, R.; Yilmaz, H.; Koper, M. T. M.; Mul, G., Manipulating the Hydrocarbon Selectivity of Copper Nanoparticles in CO₂ Electroreduction by Process Conditions. *Chemelectrochem* **2015**, *2* (3), 354-358.
- 18. David, R.; Mark, M.; Chao, W., Mass transport modelling for the electroreduction of CO₂ on Cu nanowires. *Nanotechnology* **2018**, *29* (4), 044001.
- 19. Singh, M. R.; Kwon, Y.; Lum, Y.; Ager, J. W.; Bell, A. T., Hydrolysis of Electrolyte Cations Enhances the Electrochemical Reduction of CO₂ over Ag and Cu. *J. Am. Chem. Soc.* **2016**, *138* (39), 13006-13012.

- 20. Raciti, D.; Mao, M.; Park, J. H.; Wang, C., Mass transfer effects in CO₂ reduction on Cu nanowire electrocatalysts. *Catal. Sci. Technol.* **2018**, *8* (9), 2364-2369.
- 21. Ren, D.; Fong, J. H.; Yeo, B. S., The effects of currents and potentials on the selectivities of copper toward carbon dioxide electroreduction. *Nat. Commun.* **2018**, *9*.
- 22. Lu, Q.; Rosen, J.; Zhou, Y.; Hutchings, G. S.; Kimmel, Y. C.; Chen, J. G. G.; Jiao, F., A selective and efficient electrocatalyst for carbon dioxide reduction. *Nat. Commun.* **2014,** *5*.
- 23. Dinh, C. T.; Burdyny, T.; Kibria, M. G.; Seifitokaldani, A.; Gabardo, C. M.; de Arquer, F. P. G.; Kiani, A.; Edwards, J. P.; De Luna, P.; Bushuyev, O. S.; Zou, C. Q.; Quintero-Bermudez, R.; Pang, Y. J.; Sinton, D.; Sargent, E. H., CO₂ electroreduction to ethylene via hydroxide-mediated copper catalysis at an abrupt interface. *Science* **2018**, *360* (6390), 783-787.
- 24. Hoang, T. T. H.; Verma, S.; Ma, S.; Fister, T. T.; Timoshenko, J.; Frenkel, A. I.; Kenis, P. J. A.; Gewirth, A. A., Nanoporous Copper–Silver Alloys by Additive-Controlled Electrodeposition for the Selective Electroreduction of CO₂ to Ethylene and Ethanol. *J. Am. Chem. Soc.* **2018**, *140* (17), 5791-5797.
- 25. Raciti, D.; Wang, Y.; Park, J. H.; Wang, C., Three-Dimensional Hierarchical Copper-Based Nanostructures as Advanced Electrocatalysts for CO₂ Reduction. *ACS Appl. Energy Mater.* **2018**, *1* (6), 2392-2398.
- 26. Barton Cole, E.; Lakkaraju, P. S.; Rampulla, D. M.; Morris, A. J.; Abelev, E.; Bocarsly, A. B., Using a One-Electron Shuttle for the Multielectron Reduction of CO₂ to Methanol: Kinetic, Mechanistic, and Structural Insights. *J. Am. Chem. Soc.* **2010**, *132* (33), 11539-11551.
- 27. Cao, Z.; Kim, D.; Hong, D. C.; Yu, Y.; Xu, J.; Lin, S.; Wen, X. D.; Nichols, E. M.; Jeong, K.; Reimer, J. A.; Yang, P. D.; Chang, C. J., A Molecular Surface Functionalization Approach to Tuning Nanoparticle Electrocatalysts for Carbon Dioxide Reduction. *J. Am. Chem. Soc.* **2016**, *138* (26), 8120-8125.
- 28. Wang, Z. J.; Wu, L. N.; Sun, K.; Chen, T.; Jiang, Z. H.; Cheng, T.; Goddard, W. A., Surface Ligand Promotion of Carbon Dioxide Reduction through Stabilizing Chemisorbed Reactive Intermediates. *J. Phys. Chem. Lett.* **2018**, *9* (11), 3057-3061.
- 29. Schouten, K. J. P.; Gallent, E. P.; Koper, M. T. M., The influence of pH on the reduction of CO and CO₂ to hydrocarbons on copper electrodes. *J. Electroanal. Chem.* **2014**, *716*, 53-57.
- 30. Ooka, H.; Figueiredo, M. C.; Koper, M. T. M., Competition between Hydrogen Evolution and Carbon Dioxide Reduction on Copper Electrodes in Mildly Acidic Media. *Langmuir* **2017**, *33* (37), 9307-9313.
- 31. Wang, L.; Nitopi, S. A.; Bertheussen, E.; Orazov, M.; Morales-Guio, C. G.; Liu, X. Y.; Higgins, D. C.; Chan, K. R.; Norskov, J. K.; Hahn, C.; Jaramillo, T. F., Electrochemical Carbon Monoxide Reduction on Polycrystalline Copper: Effects of Potential, Pressure, and pH on Selectivity toward Multicarbon and Oxygenated Products. *ACS Catal.* **2018**, *8* (8), 7445-7454.
- 32. Gabardo, C. M.; Seifitokaldani, A.; Edwards, J. P.; Dinh, C. T.; Burdyny, T.; Kibria, M. G.; O'Brien, C. P.; Sargent, E. H.; Sinton, D., Combined high alkalinity and pressurization enable efficient CO₂ electroreduction to CO. *Energy Environ. Sci.* **2018**, *11* (9), 2531-2539.
- 33. Whipple, D. T.; Finke, E. C.; Kenis, P. J. A., Microfluidic Reactor for the Electrochemical Reduction of Carbon Dioxide: The Effect of pH. *Electrochem. Solid-State Lett.* **2010**, *13* (9), D109-D111.
- 34. Ripatti, D. S.; Veltman, T. R.; Kanan, M. W., Carbon Monoxide Gas Diffusion Electrolysis that Produces Concentrated C₂ Products with High Single-Pass Conversion. *Joule* **2018**, DOI: 10.1016/j.joule.2018.10.007.
- 35. Mistry, H.; Behafarid, F.; Reske, R.; Varela, A. S.; Strasser, P.; Roldan Cuenya, B., Tuning Catalytic Selectivity at the Mesoscale via Interparticle Interactions. *ACS Catal.* **2016**, *6* (2), 1075-1080.
- 36. Wang, X.; Varela, A. S.; Bergmann, A.; Kühl, S.; Strasser, P., Catalyst Particle Density Controls Hydrocarbon Product Selectivity in CO₂ Electroreduction on CuO_x. *ChemSusChem* **2017**, *10* (22), 4642-4649.

- 37. Singh, M. R.; Goodpaster, J. D.; Weber, A. Z.; Head-Gordon, M.; Bell, A. T., Mechanistic insights into electrochemical reduction of CO₂ over Ag using density functional theory and transport models. *Proc. Natl. Acad. Sci. U. S. A.* **2017**, *114* (42), E8812-E8821.
- 38. Guo, H. Z.; Chen, Y. Z.; Cortie, M. B.; Liu, X.; Xie, Q. S.; Wang, X.; Peng, D. L., Shape-Selective Formation of Monodisperse Copper Nanospheres and Nanocubes via Disproportionation Reaction Route and Their Optical Properties. *J. Phys. Chem. C* **2014**, *118* (18), 9801-9808.
- 39. Li, D. G.; Wang, C.; Tripkovic, D.; Sun, S. H.; Markovic, N. M.; Stamenkovic, V. R., Surfactant Removal for Colloidal Nanoparticles from Solution Synthesis: The Effect on Catalytic Performance. *ACS Catal.* **2012**, *2* (7), 1358-1362.
- 40. Kim, D.; Xie, C. L.; Becknell, N.; Yu, Y.; Karamad, M.; Chan, K.; Crumlin, E. J.; Norskov, J. K.; Yang, P. D., Electrochemical Activation of CO₂ through Atomic Ordering Transformations of AuCu Nanoparticles. *J. Am. Chem. Soc.* **2017**, *139* (24), 8329-8336.
- 41. Huang, J. F.; Hormann, N.; Oveisi, E.; Loiudice, A.; De Gregorio, G. L.; Andreussi, O.; Marzari, N.; Buonsanti, R., Potential-induced nanoclustering of metallic catalysts during electrochemical CO₂ reduction. *Nat. Commun.* **2018**, *9*.
- 42. Roberts, F. S.; Kuhl, K. P.; Nilsson, A., High Selectivity for Ethylene from Carbon Dioxide Reduction over Copper Nanocube Electrocatalysts. *Angew. Chem. Int. Ed.* **2015**, *54* (17), 5179-5182.
- 43. Wang, Z. N.; Yang, G.; Zhang, Z. R.; Jin, M. S.; Yin, Y. D., Selectivity on Etching: Creation of High-Energy Facets on Copper Nanocrystals for CO₂ Electrochemical Reduction. *Acs Nano* **2016**, *10* (4), 4559-4564.
- 44. Loiudice, A.; Lobaccaro, P.; Kamali, E. A.; Thao, T.; Huang, B. H.; Ager, J. W.; Buonsanti, R., Tailoring Copper Nanocrystals towards C₂ Products in Electrochemical CO₂ Reduction. *Angew. Chem. Int. Ed. Engl.* **2016**, *55* (19), 5789-5792.
- 45. Grosse, P.; Gao, D. F.; Scholten, F.; Sinev, I.; Mistry, H.; Roldan Cuenya, B., Dynamic Changes in the Structure, Chemical State and Catalytic Selectivity of Cu Nanocubes during CO₂ Electroreduction: Size and Support Effects. *Angew. Chem. Int. Ed. Engl.* **2018**, *57* (21), 6192-6197.
- 46. Ma, S. C.; Sadakiyo, M.; Luo, R.; Heima, M.; Yamauchi, M.; Kenis, P. J. A., One-step electrosynthesis of ethylene and ethanol from CO₂ in an alkaline electrolyzer. *J. Power Sources* **2016**, *301*, 219-228.
- 47. Hall, A. S.; Yoon, Y.; Wuttig, A.; Surendranath, Y., Mesostructure-Induced Selectivity in CO₂ Reduction Catalysis. *J. Am. Chem. Soc.* **2015**, *137* (47), 14834-14837.
- 48. Raciti, D.; Mao, M.; Park, J. H.; Wang, C., Local pH Effect in the CO₂ Reduction Reaction on High-Surface-Area Copper Electrocatalysts. *J. Electrochem. Soc.* **2018**, *165* (10), F799-F804.
- 49. Xia, C.; Zhu, P.; Jiang, Q.; Pan, Y.; Liang, W.; Stavitsk, E.; Alshareef, H. N.; Wang, H., Continuous production of pure liquid fuel solutions via electrocatalytic CO₂ reduction using solid-electrolyte devices. *Nat. Energy* **2019**.
- 50. Gabardo, C. M.; O'Brien, C. P.; Edwards, J. P.; McCallum, C.; Xu, Y.; Dinh, C.-T.; Li, J.; Sargent, E. H.; Sinton, D., Continuous Carbon Dioxide Electroreduction to Concentrated Multi-carbon Products Using a Membrane Electrode Assembly. *Joule* **2019**.
- 51. Fletcher, S., *The Anodic Oxidation of Copper Amalgam and Polycrystalline Copper Electrodes in LiOH Solution*. 1978; Vol. 125.
- 52. Strehblow, H.-H.; Maurice, V.; Marcus, P., *Initial and later stages of anodic oxide formation on Cu, chemical aspects, structure and electronic properties.* 2001; Vol. 46, p 3755-3766.
- 53. Raciti, D.; Livi, K. J.; Wang, C., Highly Dense Cu Nanowires for Low-Overpotential CO₂ Reduction. *Nano Lett.* **2015**, *15* (10), 6829-6835.
- 54. Calle-Vallejo, F.; Koper, M. T. M., Theoretical Considerations on the Electroreduction of CO to C₂ Species on Cu(100) Electrodes. *Angew. Chem. Int. Ed.* **2013**, *52* (28), 7282-7285.
- 55. Montoya, J. H.; Shi, C.; Chan, K.; Norskov, J. K., Theoretical Insights into a CO Dimerization Mechanism in CO₂ Electroreduction. *J. Phys. Chem. Lett.* **2015**, *6* (11), 2032-2037.

- 56. Cheng, T.; Xiao, H.; Goddard, W. A., Free-Energy Barriers and Reaction Mechanisms for the Electrochemical Reduction of CO on the Cu(100) Surface, Including Multiple Layers of Explicit Solvent at pH 0. *J. Phys. Chem. Lett.* **2015**, *6* (23), 4767-4773.
- 57. Goodpaster, J. D.; Bell, A. T.; Head-Gordon, M., Identification of Possible Pathways for C-C Bond Formation during Electrochemical Reduction of CO₂: New Theoretical Insights from an Improved Electrochemical Model. *J. Phys. Chem. Lett.* **2016**, *7* (8), 1471-1477.
- 58. Schouten, K. J. P.; Pérez Gallent, E.; Koper, M. T. M., The influence of pH on the reduction of CO and CO2 to hydrocarbons on copper electrodes. *Journal of Electroanalytical Chemistry* **2014**, *716*, 53-57.
- 59. Luc, W.; Fu, X.; Shi, J.; Lv, J.-J.; Jouny, M.; Hee Ko, B.; Xu, Y.; Tu, Q.; Hu, X.; Wu, J.; Yue, Q.; Liu, Y.; Jiao, F.; Kang, Y., Two-dimensional copper nanosheets for electrochemical reduction of carbon monoxide to acetate. *Nat. Catal.* **2019**, 1.
- 60. Hahn, C.; Hatsukade, T.; Kim, Y.-G.; Vailionis, A.; Baricuatro, J. H.; Higgins, D. C.; Nitopi, S. A.; Soriaga, M. P.; Jaramillo, T. F., Engineering Cu surfaces for the electrocatalytic conversion of CO₂: Controlling selectivity toward oxygenates and hydrocarbons. *Proc. Natl. Acad. Sci. U. S. A.* **2017**, *114* (23), 5918.
- 61. Yoo, J. S.; Christensen, R.; Vegge, T.; Nørskov, J. K.; Studt, F., Theoretical Insight into the Trends that Guide the Electrochemical Reduction of Carbon Dioxide to Formic Acid. *ChemSusChem* **2016**, *9* (4), 358-363.
- 62. Durand, W. J.; Peterson, A. A.; Studt, F.; Abild-Pedersen, F.; Nørskov, J. K., Structure effects on the energetics of the electrochemical reduction of CO₂ by copper surfaces. *Surf. Sci.* **2011**, *605* (15), 1354-1359.
- 63. Li, C. W.; Kanan, M. W., CO₂ Reduction at Low Overpotential on Cu Electrodes Resulting from the Reduction of Thick Cu₂O Films. *J. Am. Chem. Soc.* **2012**, *134* (17), 7231-7234.
- 64. Cao, L.; Raciti, D.; Li, C.; Livi, K. J. T.; Rottmann, P. F.; Hemker, K. J.; Mueller, T.; Wang, C., Mechanistic Insights for Low-Overpotential Electroreduction of CO₂ to CO on Copper Nanowires. *ACS Catal.* **2017**, *7* (12), 8578-8587.

